

INFORMATION TO USERS

This manuscript has been reproduced from the microfilm master. UMI films the text directly from the original or copy submitted. Thus, some thesis and dissertation copies are in typewriter face, while others may be from any type of computer printer.

The quality of this reproduction is dependent upon the quality of the copy submitted. Broken or indistinct print, colored or poor quality illustrations and photographs, print bleedthrough, substandard margins, and improper alignment can adversely affect reproduction.

In the unlikely event that the author did not send UMI a complete manuscript and there are missing pages, these will be noted. Also, if unauthorized copyright material had to be removed, a note will indicate the deletion.

Oversize materials (e.g., maps, drawings, charts) are reproduced by sectioning the original, beginning at the upper left-hand corner and continuing from left to right in equal sections with small overlaps.

Photographs included in the original manuscript have been reproduced xerographically in this copy. Higher quality 6" x 9" black and white photographic prints are available for any photographs or illustrations appearing in this copy for an additional charge. Contact UMI directly to order.

ProQuest Information and Learning
300 North Zeeb Road, Ann Arbor, MI 48106-1346 USA
800-521-0600

UMI[®]

PREVIEW

Solid State NMR: Theoretical and Experimental Investigations

by

Paolo Rossi

A DISSERTATION

Presented to the Faculty of
The Graduate College at the University of Nebraska

In Partial Fulfillment of Requirements

For the Degree of Doctor of Philosophy

Major: Chemistry

Under the Supervision of Professor Gerard S. Harbison

Lincoln, Nebraska

August, 2001

UMI Number: 3022659

UMI[®]

UMI Microform 3022659

Copyright 2001 by Bell & Howell Information and Learning Company.

All rights reserved. This microform edition is protected against
unauthorized copying under Title 17, United States Code.

Bell & Howell Information and Learning Company
300 North Zeeb Road
P.O. Box 1346
Ann Arbor, MI 48106-1346

DISSERTATION TITLE

Solid-State NMR: Theoretical and Experimental Investigations


BY

Paolo Rossi

SUPERVISORY COMMITTEE:

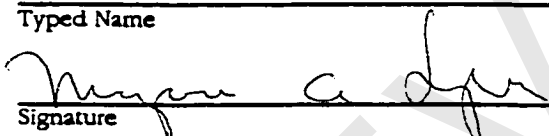
APPROVED

DATE


Signature

Gerard Harbison
Typed Name

8/2/01


Signature

Marjorie Langell
Typed Name

8/3/01


Signature

Xiao Cheng Zeng
Typed Name

8/2/01


Signature

Paul Blum
Typed Name

8/2/1


Signature

David Berkowitz
Typed Name

8/2/01

Signature

Typed Name



GRADUATE COLLEGE
UNIVERSITY OF NEBRASKA

Solid State NMR: Theoretical and Experimental Investigations

Paolo Rossi, Ph.D.

University of Nebraska, 2001

Adviser: Gerard S. Harbison

Solid-state NMR is a valuable tool for structural studies since it provides the means to acquire spectra that correspond to single conformations, in contrast to the conformational averages seen by solution NMR methods. In this thesis, the observable NMR properties are correlated to structure and dynamics of molecules in the solid state. The chemical shift and quadrupolar interactions are measured and calculated for the ^{13}C , the ^2H , and the ^{207}Pb nuclei in a variety of biological and inorganic systems.

A correlation between the isotropic ^{13}C chemical shift and the conformation is found in RNA nucleotides and nucleosides. The distinct effects of sugar puckering on the $\text{C1}'$, $\text{C4}'$, and $\text{C5}'$ resonances of $\text{C2}'$ *endo* (S type) and $\text{C3}'$ *endo* (N type) furanoid conformations allow us to separate them into two groups. Further analysis of each group reveals an additional dependence of the $\text{C1}'$ and $\text{C5}'$ resonances on the glycosidic and $\text{C4}'$ - $\text{C5}'$ exocyclic torsion angles respectively.

The asymmetry parameters and quadrupole coupling constants of the H-bonded deuteron in sodium hydrogen bis(4-nitrophenoxide) dihydrate are analyzed as a function of temperature. The electric field gradient of the strongly hydrogen-bonded deuteron is highly unusual, with a quadrupole coupling constant of less than 100 kHz over the range

213 K and 333 K. This anomalous decrease is attributed to a shortening of the O---O distance as the temperature of the crystal is lowered, resulting in a lengthening of the nominal O-D single bond.

Structural changes of PbZrO_3 have been monitored using the ^{207}Pb chemical shift. The two distinct lead sites show rather different behavior as a function of temperature. The less shielded lead maintains an almost constant asymmetry parameter $\eta = 0.2$ from 173 K to 503 K while the more shielded lead resonance becomes more axially symmetric as the temperature is raised going from $\eta = 0.199$ at 173K to $\eta = 0$ at 443 K. Powder pattern singularities remain distinct near the phase transitions, and the temperature dependence of the chemical shift tensor principal values remains continuous. That is evidence that a first order transition to a higher-symmetry phase is not present.

Acknowledgements

I would like to thank my adviser Professor Gerard Harbison. His focus, sense of direction, and the harmony he was able to create in the laboratory have made my graduate career a growing experience from both a scientific and personal standpoint.

I would also like to thank the members of my committee (in alphabetic order) Professors David Berkowitz, Paul Blum, Marjorie Langell, and Xiao Cheng Zeng for the interest they showed in my research progress. Although we did not see each other frequently, I highly regard them and I will always remember them dearly.

To my colleagues David Bussian, Joanna Clark, Mattew Dvorak, Kristin Fulton, Chunlei Guo, Bruno Herreros, Young-Sik Kye, and Xingang Xiao I give my most sincere thanks for helping me to deal with the daily grind. I wish them all the best in their future endeavors.

Special thanks to Dr. Richard Shoemaker for his help, support, NMR advice, and tutelage.

Table of Contents

Chapter 1

Survey and Synopsis

.....	1
References	13

Chapter 2

Dependence of ^{13}C NMR Chemical Shifts on Conformations of RNA

Nucleosides and Nucleotides

Summary	15
2.1 Introduction	17
2.2 Data Analysis	20
2.3 Results and Discussion	24
2.3.1 Exocyclic Torsion Angle.....	24
2.3.2 Glycosidic Torsion Angle.....	25
2.3.3 Limitations of the Present work.....	26
2.3.4 Comparison with Published Solution NMR Structures	27
References	29
Figures	32

Chapter 3

Calculation of ^{13}C Chemical Shifts in RNA Nucleosides: Structure - ^{13}C

Chemical Shift Relationships

Summary	37
3.1 Introduction	39
3.2 Method and Results	43
3.2.1 Computations.....	43
3.2.2 Statistical Analysis.....	51
3.3 Discussion	54
References	59
Tables	63
Figures	72

Chapter 4

Methylene-Only Subspectra in ^{13}C CPMAS Using a New Double

Quantum Filtering Sequence

Summary	88
4.1 Introduction	90

4.2 Results and Discussion	92
4.3 Conclusion	96
References	97
Figures	99

Chapter 5

Deuterium NMR of (D₅)-Sodium Hydrogen Bis (4-Nitrophenoxide)

Dihydrate: an Experimental and Theoretical Study

Summary	110
5.1 Introduction	112
5.2 Theory	118
5.2.1 Deuterium NMR.....	118
5.2.2 <i>Ab Initio</i> Calculation of the EFG Tensor.....	120
5.2.3 Dynamically Averaged NMR Properties of Deuterium.....	122
5.3 Method and Results	125
5.4 Discussion	133
References	138
Tables	143
Figures	147
Appendix	166

Chapter 6

²⁰⁷Pb NMR Study of Lead Zirconate and Lead Zirconate-Titanate Solid Solutions

Summary	167
6.1 Introduction	169
6.2 Materials and Methods	172
6.3 Results and Discussion	174
6.3.1 Variable-temperature ²⁰⁷ Pb NMR of lead zirconium oxide (PZ)	174
6.3.2 ²⁰⁷ Pb NMR of PbZr _{1-x} Ti _x O ₃ (PZT) solid solutions	176
6.3.3 NMR versus X-ray diffraction	177
References	178
Tables	181
Figures	184

List of Tables

Table 3-1 Average Nucleoside Structural Parameters	63
Table 3-2 Calculated CS Tensor (Average Structures B3LYP)	65
Table 3-3 Calculated CS Tensor (Average Structures B3PW91)	66
Table 3-4 Calculated CS Tensor (Common Crystalline Structures)	67
Table 3-5 Calculated CS Tensor (Rare Crystalline Structures)	68
Table 3-6 Absolute Diff. Calculated vs. Average Experimental	70
Table 3-7 Canonical Scores	71
Table 5-1 Experimental QCC , η and distances vs. temperature	143
Table 5-2 Average QCC , η vs. O-O distance (HF method)	144
Table 5-3 Average QCC , η vs. O-O distance (B3LYP method)	145
Table 5-4 Average QCC , η vs. O-O distance (MCSCF method)	146
Table 6-1 Principal Values of the Shift Tensor in PZ	181
Table 6-2 Isotropic, CSA, and Asymmetry Parameter in PZ	182
Table 6-3 Pb-O Distance vs. ^{207}Pb Chemical Shift	183

List of Figures

Figure 2-1 Structural parameters and ribose carbon numbering	32
Figure 2-2 N-pucker and S-pucker pair plot	33
Figure 2-3 N/gg and N/gt pair plot.....	34
Figure 2-4 <i>can2</i> vs. <i>can1</i> plot.....	35
Figure 2-5 C2' and C3' absolute difference vs. sum plot	36
Figure 3-1 Optimized model nucleoside structure coordinates.....	72
Figure 3-2 Plot of calc. vs. exp. ^{13}C NMR CS, method comparison	81
Figure 3-3 Dihedral angle of the ribose sugar.....	82
Figure 3-4 Plot of calc. vs. exp. ^{13}C NMR chemical shift (crystalline)	83
Figure 3-5 Plot of calc. vs. exp. ^{13}C NMR chemical shift (average)	84
Figure 3-6 Plot of canonical variables, <i>can2</i> vs. <i>can1</i>	85
Figure 4-1 Pulse sequence diagrams.....	99
Figure 4-2 CPMAS CH_2/CH intensity ratio versus mixing time	100
Figure 4-3 Optimization of the DQCP(PI) sequence	101
Figure 4-4 Comparison of DQ filtered spectra and CPMAS (tyr-HCl sample).....	102
Figure 4-5 DQCP(PI) mixing time optimization (ser sample).....	104
Figure 4-6 CPMAS vs. DQCP(PI) comparison (met sample)	106
Figure 4-7 Cholesteryl acetate backbone carbons numbering	107
Figure 4-8 CPMAS vs. DQCP(PI) comparison (cholesteryl acetate sample).....	108
Figure 5-1 X-ray structure of sodium hydrogen bis (4-nitrophenoxide) dihydrate ..	147
Figure 5-2 Deuterium Zeeman eigenstates and static spectrum.....	148

Figure 5-3 Sample deuterium NMR spectra	150
Figure 5-4 Plots of QCC and η vs. temperature	152
Figure 5-5 Water-hydroxy cluster	153
Figure 5-6 Potential function for (O-H-O) vibration	154
Figure 5-7 Wavefunction and probability density function	156
Figure 5-8 Energy level vs. O-O distance	159
Figure 5-9 Plot of EFG elements vs. H position	161
Figure 5-10 Calculated QCC and η vs. O-O distance	162
Figure 6-1 Schematic Perovskite Structure in PZT	184
Figure 6-2 X-Ray Diffractograms of PZT	185
Figure 6-3 Sample Static Spectrum of PZ	186
Figure 6-4 Static ^{207}Pb NMR spectra at 173 K to 523 K	187
Figure 6-5 Plot of Isotropic Shift, η and CSA vs. Temperature	190
Figure 6-6 MAS Spectra of PZ at 302 K and 358 K	192
Figure 6-7 Static ^{207}Pb NMR of PZT Solid Solutions at 298 K	193

Chapter 1

Survey and Synopsis

The discovery of nuclear magnetism¹ in the 1920s marked the beginning of a new era in spectroscopy. Once considered a scientific curiosity, nuclear magnetic resonance, or NMR, has undergone a remarkable evolution into one of the most widely used analytical technique in science.² The range of applicability of NMR techniques in the broad fields of chemistry, physics, and medicine is virtually limitless. The progress has been such that NMR and X-ray diffraction are now the only techniques available to obtain atomically resolved structures of biomolecules.³ Unlike X-ray, where a crystal must be obtained, NMR has great flexibility in terms of sample requirements and is an invaluable tool for the study of interfacial systems such as membrane proteins and surface

interactions.⁴ These latter systems in particular can be studied by solid state NMR. The principal experimental technique used for this thesis, solid state NMR is a versatile tool for the investigation of basic physical properties, structural and dynamic information in a wide range of organic, inorganic and biological materials in both the crystalline and the amorphous forms.

Unlike liquid state NMR where only the isotropic interactions remain in the spectrum, the intrinsic anisotropic nature of solids is such that a wider range of nuclear-electron and nuclear-nuclear coupling interactions are maintained. While that, at times, complicates the spectrum beyond what is considered interpretable, the presence of all the anisotropic information can furnish much greater detail about the system under study. With the aid of many clever techniques the shortcomings of solid state NMR can be resolved, the resolution can be improved, and specific interactions can be isolated and studied.⁵

A brief introduction on the fundamental interactions in NMR that are applicable to the work done in this thesis will be given in this chapter together with the general literature references. Following that a short summary of the techniques that were employed and finally a brief description of the contents of each chapter and the underlying motivations for the work. Specific literature references will be given in each chapter of the thesis.

In quantum mechanics the observable interactions in NMR are the eigenvalues of the total nuclear Hamiltonian (H).^{6,7} The total Hamiltonian can be separated into the sum of the dominant Zeeman Hamiltonian (H_Z) and the fine interaction terms as follows:

$$H = H_Z + H_{CS} + H_D + H_J + H_Q \quad (1)$$

where H_{CS} , H_D , H_J , and H_Q are the chemical shift, dipolar, J-coupling, and quadrupolar Hamiltonian, respectively. The Zeeman Hamiltonian is the most basic nuclear Hamiltonian, and is the result of the coupling of the intrinsic magnetic dipole moment of nuclei with non zero spin quantum number ($I \geq 1/2$) with an external magnetic field \mathbf{B}_0 . This dipole moment is given by:

$$\mu = \gamma \hbar I \quad (2)$$

where γ is another intrinsic property of the nucleus called the gyromagnetic ratio, and I is the spin operator, a 2×2 and 3×3 matrix for the spin $1/2$ and spin 1 nucleus, respectively.

By convention the \mathbf{B}_0 field is oriented in the z direction and the Zeeman Hamiltonian takes the form:

$$H_Z = -\mu \cdot \mathbf{B}_0 = -\gamma \hbar \mathbf{B}_0 I_Z \quad (3)$$

The number of allowed energy transitions for the Zeeman Hamiltonian again depends upon the value of I . For $I = 1/2$ there is one energy transition between two levels at angular frequency:

$$\omega_0 = 2\pi f_0 = \gamma \mathbf{B}_0 \quad (4)$$

The resonance frequency ω_0 which is also called the Larmor frequency is characteristic for each nucleus.

The chemical shift (or chemical shielding) Hamiltonian accounts for what happens to nuclei that are surrounded by electrons when under the influence of an external field. The distribution of electric currents around the nuclei causes additional magnetic fields to be created. The intensity of these fields is generally much lower than the external field \mathbf{B}_0 and they produce small shifts in the resonance frequencies. The sign of this shift may be positive or negative depending on whether the field has the same sign or opposite sign to \mathbf{B}_0 . The chemical shift Hamiltonian has the expression:

$$H_{CS,j} = I_j \sigma_j \mathbf{B}_0 \quad (5)$$

The chemical shift tensor of the j spin, σ_j , is a rank 2 tensor that expresses the coupling of the spin to the local induced magnetic environment. In the secular form this local magnetic field is given by:

$$B_{\sigma,j} = \sigma_{zz}^{LAB} B_0 \quad (6)$$

The laboratory frame and the principal axis system (PAS) frame, that is the frame of the diagonalized tensor, are related by a set of rotations about the Euler angles α and β that define a rotation in 3D space. So σ_{zz} becomes:

$$\sigma_{\pm} = \sigma_{iso} + \frac{\Delta\sigma}{3} \left[(3 \cos^2 \beta - 1) + \eta \sin^2 \beta \cdot \cos^2 \alpha \right] \quad (7)$$

where σ_{iso} is the trace of the chemical shift tensor, $\Delta\sigma$ is the chemical shift anisotropy and η is the asymmetry parameter. The definitions for the latter two quantities are:

$$\Delta\sigma = \frac{3}{2}(\sigma_{\pm} - \sigma_{iso}) \text{ and } \eta = (\sigma_{yy} - \sigma_{xx})/(\sigma_{\pm} - \sigma_{iso}) \quad (8)$$

The shielding is proportional to the strength of B_0 . It is generally measured in parts per million (ppm) relative to a standard reference rather than as an absolute quantity. The shielding tensor can be decomposed into the sum of an axially symmetric and an axially asymmetric tensor. The symmetric part can be diagonalized to give the three principal values that are observable in solid state NMR but that collapse into a single isotropic (average) value in liquid state NMR.

The dipolar Hamiltonian represents the coupling between the magnetic dipole moments of two nuclei in space. The interaction of the spin j and k separated by a distance r is:

$$H_{D,jk} = \frac{\gamma_j \gamma_k \hbar}{r_{jk}^3} \frac{1}{2} (3 \cos^2 \theta_{jk} - 1) \left[2I_{jz}I_{kz} - \frac{1}{2}(I_{+j}I_{-k} + I_{-j}I_{+k}) \right] \quad (9)$$

The form of Eq. 9 is important because it contains the θ_{jk} angle which is the angle between the magnetic field B_0 and the vector connecting the j and k spins. As a result, the dipolar Hamiltonian can be averaged out by tilting the axis of the sample with respect to

B_0 by an angle equal to $\arccos(1/\sqrt{3})=54.7^\circ$ and by simultaneously spinning the sample about this tilted axis. This is the basis of the technique called magic angle spinning (MAS).⁸ Eq. 9 can be simplified by removing the terms that do not commute with the Zeeman Hamiltonian:

$$H_{D,jk} = 2\gamma_j\gamma_k\hbar\mathbf{I}_j \cdot \mathbf{D} \cdot \mathbf{I}_k \quad (10)$$

In this form the dipolar tensor \mathbf{D} is displayed. Unlike the chemical shift tensor (CS), this tensor is axially symmetric and traceless with principal values that are functions of r^{-3} . As stated above dipolar interactions are an important source of line broadening in the solid state but they average out in liquid state NMR.

An additional type of interaction between two spins is the J -coupling or scalar coupling interaction. This type of coupling is generated by two nuclei interacting through their bonding electrons, and therefore the interaction is purely intramolecular. This definition has to be somewhat revised after the recent measurement of through H-bond J -coupling.⁹ Thus, intermolecular interactions that include a degree of covalent bond character should be included. The Hamiltonian for this interaction is as follows:

$$H_{J,jk} = 2\pi\mathbf{I}_j \cdot \mathbf{J} \cdot \mathbf{I}_k \quad (11)$$

An insignificant source of broadening in the solid state, J -coupling is very important in liquid state NMR. For this reason an expression that contains only a scalar term is more convenient:

$$H_{J,jk} = 2\pi J_{jk} \mathbf{I}_j \cdot \mathbf{I}_k \quad (12)$$

The coupling constant J_{jk} is expressed in Hz.

The last interaction that will be discussed here is the quadrupolar interaction. The quadrupolar interaction pertains to the quadrupolar nuclei with spin $\neq 1/2$. These nuclei have a nonspherical nuclear charge distribution. Quadrupolar nuclei possess an intrinsic quadrupole moment Q that can either be positive or negative. The magnitude and sign of Q measure the extent of the nonspherical distortion and the direction of distortion either toward a prolate or oblate ellipsoid charge distribution, respectively. Shifting the focus on the nuclear surroundings another very important entity needs to be defined: the electric field gradient (EFG) tensor $\nabla \mathbf{E}$. The electric field gradient quantifies the non-uniform charge density around the nucleus as a result of chemical environment. The quadrupole coupling is therefore the coupling between the non-spherical nuclear charge and the surrounding electrostatic environment. A more in-depth discussion on EFG will be given in Chapter 5. The Hamiltonian for the quadrupolar interaction is written as follows:

$$\begin{aligned} H_Q &= \frac{eQ}{6I(2I-1)\hbar} \mathbf{I} \cdot \nabla \mathbf{E} \cdot \mathbf{I} \\ &\equiv \frac{eQ}{6I(2I-1)\hbar} \sum_{\alpha, \beta=x,y,z} \nabla E_{\alpha\beta} \left[\frac{3}{2} (I_\alpha I_\beta + I_\beta I_\alpha) - \delta_{\alpha\beta} I(I+1) \right] \end{aligned} \quad (13)$$

where Q is the intrinsic quadrupole moment for the nucleus, e is the proton charge, and I is the nuclear spin. The Kronecker delta, $\delta_{\alpha\beta}$, equals to 1 for $\alpha = \beta$, and to 0 for $\alpha \neq \beta$.

The electric field gradient is a symmetric and traceless rank two tensor ($\nabla E_{xx} + \nabla E_{yy} + \nabla E_{zz} = 0$) in which the principal components are ordered as follows:

$$|\nabla E_{xx}| < |\nabla E_{yy}| < |\nabla E_{zz}| \quad (14)$$

In the PAS the asymmetry parameter can be defined:

$$\eta = \frac{\nabla E_{xx} - \nabla E_{yy}}{\nabla E_{zz}} \quad (15)$$

The η value is a measure of the axial asymmetry of the tensor. The general expression for the quadrupole coupling constant is:

$$\omega_Q = \frac{3e^2qQ}{4I(2I-1)\hbar} \quad (16)$$

In this expression eq is the ∇E_{zz} component of the field gradient tensor in the PAS. The quadrupole coupling has the same angular dependence as the dipole-dipole and the chemical shift interactions; the relevant expressions will be shown in Chapter 5 for the case of deuterium. Quadrupolar interactions are very important in NMR since most nuclei in the periodic table have spin greater than 1/2. Although the most popular NMR nuclei, ^1H , ^{13}C , ^{15}N , ^{19}F , ^{31}P that are all spin 1/2 are not directly subject to quadrupolar interactions, coupling to a quadrupolar nucleus can dramatically affect their spectrum.

If all the elements of the total Hamiltonian were present simultaneously, the NMR spectrum would be broad and entirely useless. Most of the time in modern pulsed Fourier

transform NMR, only the effects of two or three interactions will be present in the spectrum. By working in the rotating frame, the Zeeman frequency is initially set in the instrument and has no other consequence. In liquid samples isotropic averaging nulls-out all the anisotropic interactions leaving only chemical shift, and J-coupling interactions. In the case of quadrupolar nuclei the predominant interaction is the large quadrupole splitting with all other interactions contributing to minor broadening of the spectrum. In the solid state, all the traceless coupling tensors disappear at ($3\cos^2\theta = 1$) (with spinning), so the chemical shift anisotropy (CSA), the dipole-dipole, and the quadrupole interactions can be removed by magic angle spinning. Heteronuclear spin couplings can be removed by decoupling techniques. Nuclei with low γ and low isotope abundance pose a sensitivity problem. Techniques were developed that employ magnetization transfer from the most sensitive nucleus (^1H) to the less sensitive. Cross-polarization (CP) techniques are based on this underlying principle.¹⁰

Static and MAS NMR were the two main techniques used for the data acquisition in this thesis. The pulse sequences ranged from the simple one-pulse, to the Hahn echo sequence, and the solid echo or quadrupole echo. While the MAS technique is very general and can be used with a variety of pulse sequences, the acronym CP MAS refers to a very specific technique in which the pulse is applied to the abundant spin and transferred to the rare spin, which is subsequently observed. This pulse sequence is discussed in detail in Chapter 4.

The one pulse ($\pi/2$ -Acq) is the simplest possible pulse sequence in which a single 90° pulse is applied to a nuclear spin and the time dependent magnetization decay is